Nanotechnology **22** (2011) 395701 (8pp) doi:10.1088/0957-4484/22/39/395701

Piezoresistance of top-down suspended Si nanowires

A Koumela[1,2], D Mercier[1], C Dupré[1], G Jourdan[1], C Marcoux[1], E Ollier[1], S T Purcell[2] and L Duraffourg[1]

[1] CEA-Leti, MINATEC Campus, 17 rue des Martyrs, 38054 Grenoble Cedex 9, France
[2] Laboratoire de Physique de la Matière Condensée et Nanostructures, Université Lyon I, CNRS, UMR 5586, Domaine Scientifique de la Doua, F-69622 Villeurbanne Cedex, France

E-mail: laurent.duraffourg@cea.fr

Received 7 April 2011, in final form 9 August 2011
Published 2 September 2011
Online at stacks.iop.org/Nano/22/395701

Abstract
Measurements of the gauge factor of suspended, top-down silicon nanowires are presented. The nanowires are fabricated with a CMOS compatible process and with doping concentrations ranging from 2×10^{20} down to 5×10^{17} cm^{-3}. The extracted gauge factors are compared with results on identical non-suspended nanowires and with state-of-the-art results. An increase of the gauge factor after suspension is demonstrated. For the low doped nanowires a value of 235 is measured. Particular attention was paid throughout the experiments to distinguishing real resistance change due to strain modulation from resistance fluctuations due to charge trapping. Furthermore, a numerical model correlating surface charge density with the gauge factor is presented. Comparison of the simulations with experimental measurements shows the validity of this approach. These results contribute to a deeper understanding of the piezoresistive effect in Si nanowires.

(Some figures in this article are in colour only in the electronic version)

1. Introduction

Suspended silicon nanowires (SNWs) are among the most popular nano-electromechanical systems (NEMSs) that are actively studied for making new highly-sensitive sensors for future experiments on mass (Yang *et al* 2006, Ilic *et al* 2004, Arcamone *et al* 2009, Jensen *et al* 2008), and force detection (Staufer *et al* 2007). However, sensitive detection of the SNW displacement remains a challenge. Several detection techniques, such as capacitive (Colinet *et al* 2009b), magnetomotive (Feng *et al* 2008), piezoresistive (Bargatin *et al* 2005, He *et al* 2008) and field-emission (Ayari *et al* 2007) transduction, have already been introduced. Magnetomotive detection typically requires large magnetic fields (2–8 T) and is thus not suitable for integrated applications. Field-emission detection demands complex instrumentation and its stability in time is difficult. Piezoresistive detection seems to offer great potential compared to capacitive detection, especially at high resonant frequencies (Mile *et al* 2010, Colinet *et al* 2009a). For this reason, it is important to investigate experimentally the piezoresistive properties of top-down fabricated silicon nanowires, both before (non-suspended) and after (suspended) the release process. The piezoresistance of silicon was first investigated by Smith (1954) and later by Kanda (1982). In bulk crystals the piezoresistance effect results from strain-induced changes in the band structure, and hence carrier populations and effective masses. The enhanced piezoresistive effect of p-type silicon compared to n-type, already observed by Smith (1954), led to further scientific research described in several publications. During the last few years, the so-called 'giant piezoresistivity' in p-doped SNW has been intensely explored. Results on top-down fabricated nanowires have already been reported but they deal with non-suspended structures (Toriyama *et al* 2001, Toriyama and Sugiyama 2002, Reck *et al* 2008, Milne *et al* 2010) with the smallest wires (width = 5 nm, thickness = 23 nm) being discussed in Barwicz *et al* (2010). Also, results on bottom-up suspended nanowires (He and Yang 2006, Lugstein *et al* 2010, Zhang *et al* 2011) have been presented. However, no results on top-down suspended nanowires have been shown so far.

There are currently two theories reported to explain the origin of the giant piezoresistance in silicon nanowires observed previously by He and Yang (2006). The first, proposed in the original article, connects the effect to the

 © 2011 IOP Publishing Ltd Printed in the UK & the USA

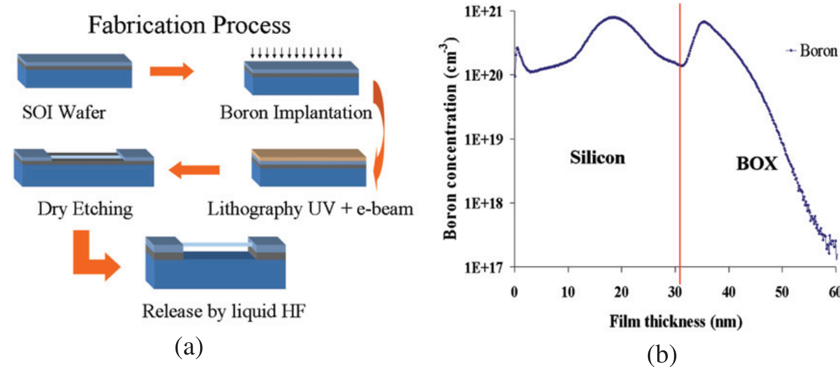

Figure 1. (a) Flow chart of the device fabrication process. (b) SIMS profile of a 2×10^{20} cm^{-3} doped wafer.

dimensions of the nanowires and suggests a mechanism based on the strain modulation of the conductance. The second theory, exposed in a series of communications published since 2008 (Rowe 2008, Barwicz *et al* 2010, Milne *et al* 2010), identifies the origin of this phenomenon in the partial depletion of the conduction channel. More precisely, Rowe (2008) proposes that the density of the trapped charges in the Si/SiO_2 interface modulates the nanowire conductance.

In this paper, a study of the gauge factor of top-down nanowires is presented, where the gauge factor is defined as the resistance variation with applied strain. Results on suspended top-down nanowires are shown for the first time. Moreover, a comparison between suspended and identical non-suspended structures is performed. Most tested nanowires had cross-sections ranging from 40 nm by 40 nm to 36 nm by 38 nm and lengths varying between 350 nm and 5 μm with one larger SNW of cross-section 50 nm by 160 nm and length 2.5 μm. The fabrication process is based entirely on microelectronic tools and is CMOS compatible. During the electrical characterization of the nanowires, conductance drift with time was monitored. In contrast to Milne *et al* (2010), the nanowire conductance is quite stable in time and there is no confusion about the extraction of the gauge factor. For the doping levels examined here (2×10^{20} down to 5×10^{17} cm^{-3}) there is no giant piezoresistance effect. However, there is a clear increase of the gauge factor measured on released nanowires with respect to the non-released structures, probably due to a difference of surface charge density. Experimental results are compared to simulations based on a theoretical model that takes into account the surface charge states. In the following sections, all these aspects are discussed in detail.

2. Fabrication process

As mentioned above, the device fabrication is based on microelectronic tools. The starting substrate is an SOI wafer oriented (100). The initial Si film thickness is 70 nm and the BOX (buried oxide) is 145 nm for the devices doped at 5×10^{17} and 2×10^{20} cm^{-3}, while for the devices doped at 1×10^{19} cm^{-3} the film thickness is 160 nm and the BOX is 400 nm. In order to obtain 40 nm thick devices, the initial Si film thickness is reduced by successive oxidation and etching steps. Afterwards, implantation and ebeam lithography for nanowire definition are performed. The activation of the dopants is made by a spike annealing at 1050 °C under N_2. The contacts are defined by DUV lithography. In the case of low doped nanowires (5×10^{17} cm^{-3}), a second implantation (1×10^{20} cm^{-3}) at the contacts is performed to reduce the contact resistance and get a good Ohmic contact. Finally, electrical pads are fabricated by AlSi deposition. The release of the nanowires is carried out by wafer immersion in liquid hydrofluoric acid (HF). The flow chart of the process is briefly described in figure 1(a) where the fabrication of the electrical pads is not shown. A SIMS (secondary ion mass spectrometry) profile (chemical concentration of boron) of a 2×10^{20} cm^{-3} doped wafer in figure 1(b) shows the dopant distribution of the wafer. A special design on silicon for SIMS acquisition was used. The boron peak at about 18.5 nm presented in the silicon film could be attributed to the amorphization of the silicon layer after implantation. In fact, for an annealing performed at 1050 °C, the solubility limit of boron in silicon is set to 1.5×10^{20} cm^{-3} (Armigliato *et al* 1977). The excess of boron atoms present in the silicon are not annealed (and thus not activated) and furthermore they do not diffuse creating the peak observed in our measurement. However, the nanowires tested contain no amorphous regions as can be seen in the TEM photograph (figure 2(b)).

In figure 2(a), a SEM (scanning electron microscopy) photograph of a typical released nanowire is shown, while in figure 2(b), a cross-section of a suspended nanowire is presented (transmission electron microscopy). It is observed that the nanowire cross-section is nearly square and that a thin oxide film has been grown on its surface.

3. Experimental part

3.1. Experimental protocol for resistance measurements

The fabricated nanowires were oriented in the ⟨110⟩ direction. All the devices were tested electrically before stress measurements in order to extract mean resistance values and to identify the functional devices to be used afterwards in piezoresistive measurements. The effective doping concentration of the devices was extracted from electrical measurements and in the case of the 2×10^{20} cm^{-3} doping the results were confirmed by the SIMS (secondary

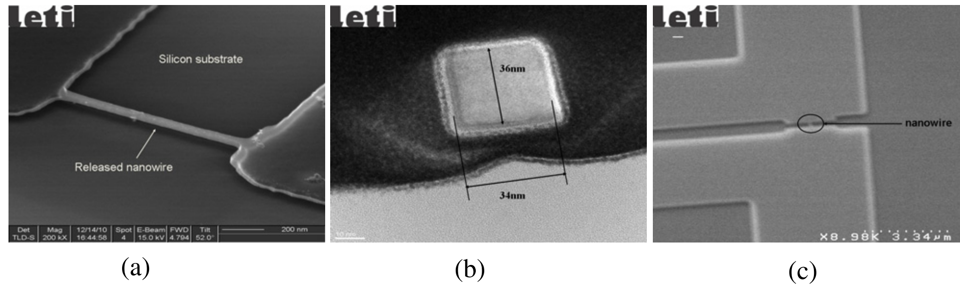

Figure 2. (a) SEM photograph of a released nanowire. (b) TEM cross-section of a released nanowire. (c) SEM photograph of the four-point probe configuration. The two vertical lines were used for polarization of the nanowire and current measurement, while the two horizontal lines were used for voltage measurement.

ion mass spectroscopy) measurements presented in figure 1(b). SIMS gives the chemical concentration of the dopant, in this case boron.

The nanowire resistances were measured either by the four-point probe method (figure 2(c)) when this configuration was available, or by the two-point probe method for low doped nanowires. In all cases, the resistance was extracted from the linear part of the I–V characteristics. In the case of the two-point probe measurements, the access resistances were determined from the plots of the measured resistances with respect to the nanowire lengths, $R(L)$. The access resistances conformed to the nanowire resistances. Experimental results gave higher resistances than theoretical calculations ($R = \rho L/S$) that cannot be explained only by the access resistance. This issue will be discussed in section 4 dedicated to the resistance and the gauge factor model.

In figure 3 the linearity of typical I–V characteristics for applied voltages in the range [−0.2 V, 0.2 V] are shown. For the results presented in this paper, the linear fitting for the extraction of the resistance is based on measurements in the range [−100 mV, 100 mV].

Figure 4 shows the dispersion of 12 similar devices fabricated on the same wafer for two different doping concentrations. A probe card mounted on an automatic prober is used for the electrical measurements on whole wafers, while metallic needle probes are employed for the strain measurements.

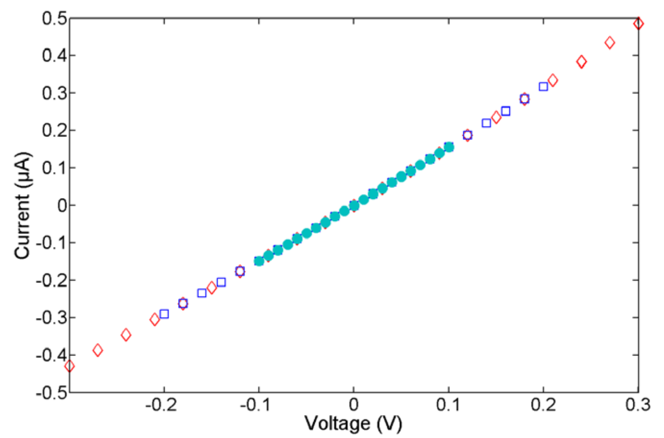

Figure 3. I–V characteristics for a device doped at 5×10^{17} cm^{-3} obtained with an HP4156C instrument. The different shapes correspond to different measurement voltage ranges ([−0.1 V, 0.1 V], [−0.2 V, 0.2 V] and [−0.3 V, 0.3 V]) for the same nanowire. The behaviour is linear and symmetric (full squares) for the measurement range [−0.1 V, 0.1 V]. However, for a higher voltage range, [−0.3 V, 0.3 V] (open diamonds), the characteristics deviate somewhat from linear and symmetric response ($I = 0.5$ μA for $V = 0.3$ V and $I = 0.42$ μA for $V = -0.3$ V). Similar observations are reported by Toriyama and Sugiyama (2002).

3.2. Experimental protocol for strain measurements

All the strain measurements were performed at room temperature with a four-point bending bench (figure 5(d)). The instrument used for the extraction of the I–V curves was an HP4156C and all the measurements shown in the following sections were made with it. Depending on the bench configuration (figures 5(a)–(c)), a series of tension or compression measurements was performed without removing the device from the bench. However, between the tension and compression measurements, the bench configuration had to be modified and the samples repositioned. Due to this procedure, the strain offset might be different for the series of tension and compression; however, only the strain variation and the relative resistance change account for the extraction of the piezoresistive coefficient and these should always be the same. The stress is generated by the vertical displacement of the two lower support cylinders. This displacement is monitored and it is used to calculate the strain applied at the device via the equation

$$\varepsilon = \frac{t}{2a(L/2 - 2/3a)} y \tag{1}$$

where t is the substrate thickness, α is the distance between the internal and external rods used for stress application, L is the distance between the two outer rods and finally y is the vertical displacement of the two lower support rods.

It should be noted that the four-point bending method is very accurate. The strain is distributed quite uniformly on the sample and the associated error depends mainly on the graduation of the vertical movement (one graduation was 10 μm), resulting in a relative error of 3.3%. Furthermore, according to Lube and Manner (1997), a large outer span (L) results in small errors of this method. This is true for the measurements presented in this paper as the span length used was about 60 mm. For more details on the four-point bending method and the errors associated with it, see also Lund and Finstad (2004) where a four-point bending bench was fabricated and tested.

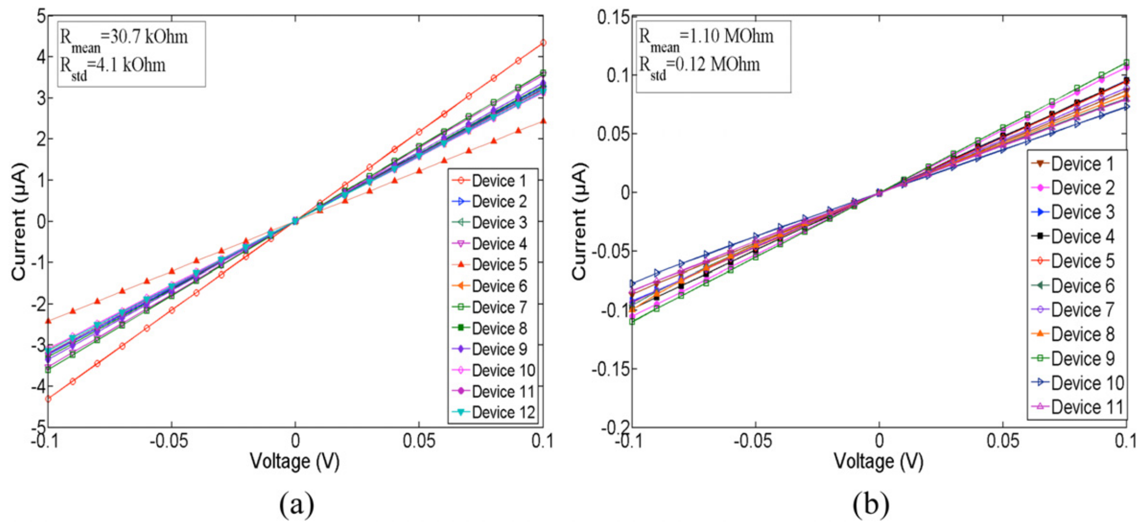

Figure 4. (a) I–V characteristics obtained with a Keithley 2400 for twelve similar devices doped at 2×10^{20} cm^{-3} (suspended nanowires) that were fabricated on the same substrate with dimensions $w = 36$ nm, $t = 38$ nm and $L = 2.53$ μm. The measurements presented here were performed in the two-point probe configuration. The mean resistance for this device was 30.7 kΩ with a standard deviation of 4.1 kΩ. (b) As in (a) but for the case of 5×10^{17} cm^{-3}. Here, the mean resistance was 1.10 MΩ with a standard deviation of 0.12 MΩ.

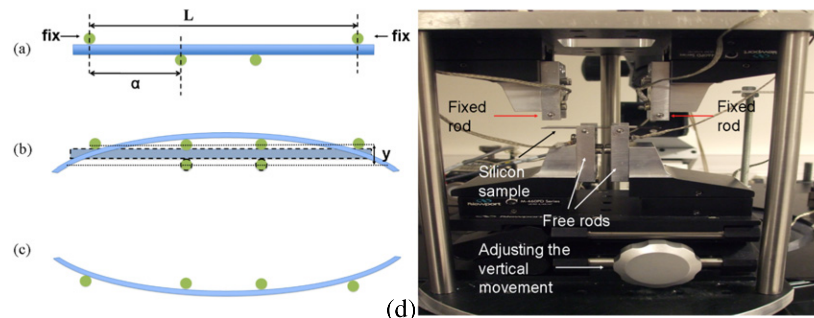

Figure 5. (a) Before applying a tensile or compressive strain, the silicon sample (2 cm wide by 6 cm long) is positioned on the support rods and a resistance measurement is performed. (b) Configuration for the application of tensile strain. (c) Configuration for the application of compressive strain. (d) Photograph of the four-point bending bench.

3.3. Measurements calibration

In order to verify the origin of the observed piezoresistance, numerous successive measurements are performed on the samples under the same strain conditions to discriminate between resistance change due to fluctuations (charge trapping) and resistance change due to strain modulation. Indeed, in a recent paper Rowe (2008) gives evidence that the apparent giant piezoresistance reported in He and Yang (2006) results from a depletion region created on the nanowire surface. In Milne *et al* (2010) it is shown that the conductance variation of the nanowires with time may lead to false results concerning the gauge factor. Actually, the gauge factor depends on the time elapsed between two resistance measurements. For the nanowires presented in this paper and for short time periods there is no significant resistance change. The proof of this is shown in figure 6 where the results of ten successive I–V characteristics of the same unstrained nanowire are plotted. The error bars are so small that there is practically no resistance change between the first and the tenth measurements. This plot is used later as a calibration curve for resistance versus strain measurements.

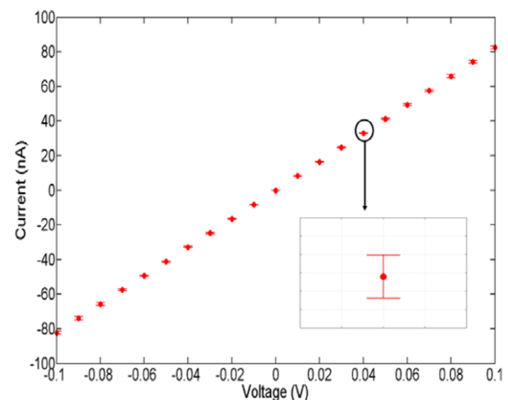

Figure 6. Calibration curve for a released nanowire doped at 5×10^{17} cm^{-3}. Each dot is the average of ten measurements. The inset at the right bottom of the figure shows a dot of this curve with the corresponding standard deviation bars. The standard deviation is smaller than the conductance variations due to strain.

Furthermore, the conductance variation, $\Delta\sigma$, is measured as a function of time. Conductance fluctuations are observed when measuring the device for 1 h and for an applied

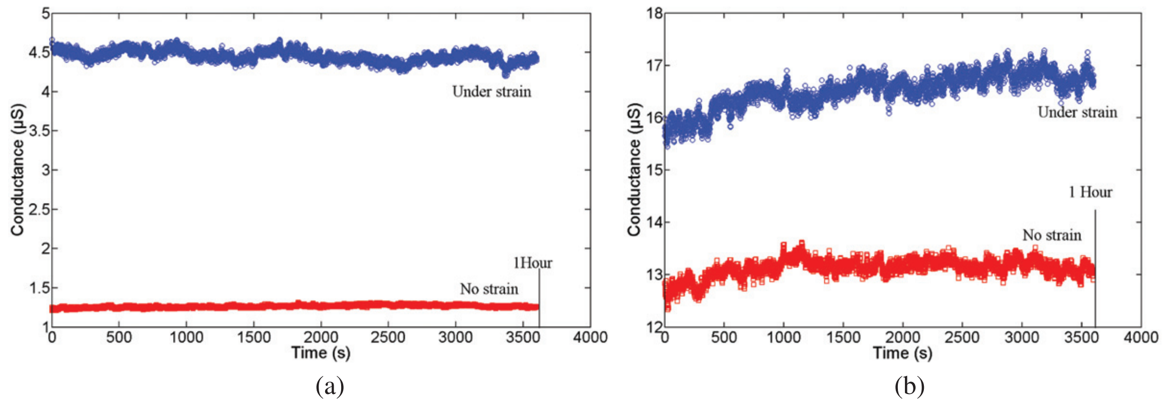

Figure 7. (a) Conductance variation measurement for released nanowires doped at 5×10^{17} cm^{-3}. (b) Conductance variation in time for released nanowires doped at 2×10^{20} cm^{-3}.

voltage of 0.1 V. Unlike Milne *et al* (2010), there is no clear abrupt conductance decrease followed by an increase. In fact, considering the measurements on low doped devices in figure 7(a), it is reasonable to assume that there is no significant error when extracting the gauge factor from the I–V characteristics taken during a short time (less than one hour). For comparison, the same measurements for highly doped nanowires (2×10^{20} cm^{-3}) are shown in figure 7(b). The relative conductance change due to strain ($\Delta G/G = 0.73$) is greater than the conductance fluctuations ($\Delta G/G = 0.10$) observed during this time period for the low doped nanowire. Similarly, for the highly doped nanowire, the conductance fluctuation is about 0.1, while the conductance change due to the applied strain is about 0.18.

Another difference between the conductance measurement presented by Milne *et al* (2010) and the protocol followed here for the extraction of the gauge factor is that the nanowires are not under constant bias. In fact, the nanowires are biased for the time it takes to plot an I–V characteristic and for the rest of the time there is no current flow. Given that the time constant for charge trapping is much smaller than 1 s, there should be no influence on the measurements.

The results presented in figure 7 along with the calibration curve (figure 6) demonstrate that the measurements are reliable and that the extracted piezoresistive coefficients are not only due to a charge trapping process.

4. Resistance and gauge model

The resistance and gauge factor of the device are calculated with a numerical tool developed in-house that takes into account the depletion effect (Seo *et al* 2006, Schmidt *et al* 2007), dopant deactivation (Diarra *et al* 2007), and the Mott transition (for high doping level). Without stress, this model provides an effective electrical cross-section s_{eff} that corresponds to the region of conduction of free charge carriers. s_{eff} instead of the physical cross-section is then used to compute the nanowire resistance. To first order, the piezoresistivity in the SNW can be considered as resulting from two additive and simultaneous processes. The first one is the bulk piezoresistivity while the second one corresponds to the depletion width modulation induced by the stress. Firstly, the bulk piezoresistivity computation uses a model presented in the paper by Richter *et al* (2008) that includes both carrier density variation and valence band distortion caused by a stress. It is then well suited to p-doped silicon compared to Kanda's model that can mainly be used for n-doped silicon. Secondly, the modulation of the depletion width is considered as linear with the stress. The surface potential slope with respect to the stress $\partial\psi/\partial\sigma$ (Rowe 2008) is then introduced to evaluate the charge carrier density change that sets the depletion width. It is set to fit the experimental data as well as possible.

Table 1. Resistance of 5×10^{17} cm^{-3} doped devices with $w = 36$ nm and $t = 38$ nm. Comparison between theory (no nanowire depletion was considered) and experiment. The uncertainty in the calculated values is about 8%.

Length (μm)	$R_{\mathrm{theoretical}} = \rho(L/S)$ (kΩ)	R_{model} (kΩ)	$R_{\mathrm{experimental}}$ (kΩ)
0.4	91.2	32	120
0.5	114	162	168
1	228	324	467
2	456	649	1060
5	1140	1621	2840

For comparison, the theoretical resistance based on the real geometrical dimensions of the nanowires determined from CD SEM (critical dimensions scanning electron microscopy) observations is calculated (table 1). Due to the high accuracy of this technique, the only uncertainty in the calculation arises from the device width dispersion. The measured width is around 36 nm with a deviation of 3 nm that results in 8% uncertainty in the theoretical resistance. Regarding the low doped devices (5×10^{17} cm^{-3}), the theoretical calculation gives lower resistance values than the experimental ones (table 1). This is not explained by the width dispersion but it may be attributed to the charge trapping that takes place in the Si/SiO_2 interface and results in partial depletion of the nanowire (Rowe 2008). The resistance calculated by the model is also given in table 1. For the diameter considered here, there is no deactivation process of the dopants but only the surface depletion mechanism. This resistance is higher than the theoretical one (except for the shorter nanowire) but still

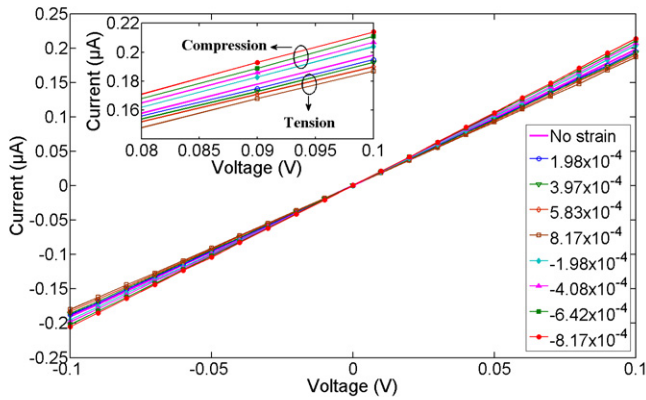

Figure 8. Typical electrical characteristics for a 5×10^{17} cm^{-3} doped nanowire with $L = 1$ μm, $w = 36$ nm and $t = 38$ nm. In the inset, the distinction of the compressive from the tensile measurements is clear.

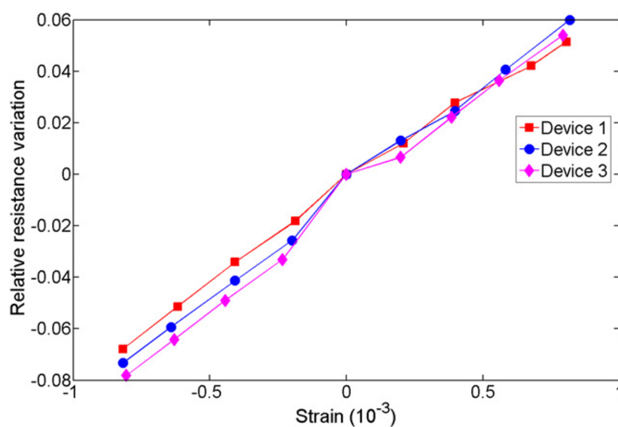

Figure 9. Resistance variation with strain of a 1 μm long, 36 nm wide and 38 nm thick nanowire doped at 5×10^{17} cm^{-3}.

lower than the experimental results. Differences between the model (ideal case) and physical cross-section could probably explain this mismatch.

In figure 10, the calculation of the gauge factor for a nanowire for various surface charge densities, N_{it}, is presented. It was not possible to extract the value of N_{it} for the tested nanowires because of the lack of an MOS configuration. Thus, charge pumping measurements were not possible. However, from previously published results (Tachi *et al* 2009) on nanowires fabricated with a similar process, the lower limit of N_{it} is set at 2.84×10^{11} cm^{-2}. In this context, the values of the surface charge density used in the model range from 1×10^{10} to 3×10^{11} cm^{-2}. Even though the calculation is not exact, as a cylindrical cross-section is considered and there is only an estimation of the surface charge density according to the literature, the predictions are rather close to the experimental values.

5. Results and discussion

Due to the use of the four-point bending method, the strain application is limited to $\leqslant$0.1%. Above this limit, the silicon

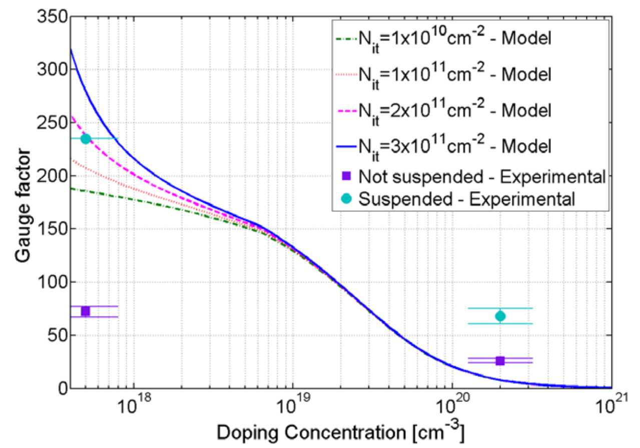

Figure 10. Comparison between simulation and experimental values of the gauge factor as a function of the doping concentration. The model gives gauge factor estimations that are close to the experimental values measured. For the calculation, an equivalent radius of 20 nm is considered.

sample breaks. The resistance increases under tension and decreases under compression similarly to earlier observations (He and Yang 2006, Barwicz *et al* 2010, Milne *et al* 2010). An increase of the gauge factor with decreasing doping concentration is observed, as expected in bulk silicon (see for instance Kanda 1982 or Richter *et al* 2008). However, giant piezoresistive coefficients up to some thousands were not observed, mainly due to the relatively high doping levels used with respect to He and Yang (2006) which eliminated time-varying charge trap effects. Moreover, concerning the extraction of the gauge factor, slight differences between the tension and compression measurements are observed. In fact, the compression measurements result in a higher gauge factor than the tension measurements (see figure 8), similarly to the trends observed in Barwicz *et al* (2010) and He and Yang (2006).

In figure 9, the relative resistance variation is plotted versus strain which allows deduction of the gauge factor. The relative resistance variations for three devices with the same geometrical and material specifications have been plotted. The plots are linear and quite reproducible, thus giving reliable gauge values.

These measurements were performed for various devices at doping levels of 2×10^{20} cm^{-3}, 1×10^{19} cm^{-3} and 5×10^{17} cm^{-3} for suspended and fixed nanowires in order to determine the corresponding gauge factors. As it is indicated in figure 10, the gauge factor depends not only on the doping level but also on whether the nanowire is suspended or not. An important increase of the gauge factor for the released nanowires is observed. In the case of the 5×10^{17} cm^{-3} doping, the increase is larger than 100%. This large difference between suspended and non-suspended nanowires cannot be attributed only to a different charge trapping procedure. The transmission of the strain, for the non-suspended nanowires, from the substrate to the nanowire is not well characterized as of yet. It is quite probable that the real strain is much smaller than the monitored one and so the gauge factor will be higher.

A comparison of the experimental results with results from the model described in the previous section is presented in figure 10. It is observed that the experimental results are close to the model values and that for the low doped suspended nanowire there is a good accordance with the model for a surface charge density of 2×10^{11} cm^{-2}, consistent with the lower estimated limit of 2.84×10^{11} cm^{-2} given above. For the large doping level, the theoretical model is reduced to Richter's one, which is suitable up to 10^{20} cm^{-3}. For larger values, the extracted gauge factors are always smaller than the experimental values.

In figure 11, the results of this work are compared to previous experimental work. The gauge factors taken from He and Yang (2006) are approximated from the graphic given in the reference. It is observed that their values for bottom-up nanowires are higher than the results presented here for suspended nanowires and other experimental work. In particular, comparing devices doped at 10^{19} cm^{-3}, the gauge factor for bottom-up nanowires is twice the gauge factor measured in this work and, similarly, the gauge factor for the doping of 10^{17} cm^{-3} is 1.5–2 times higher. This is quite interesting because it may be evidence for a difference between bottom-up and top-down nanowires. It is interesting also that the intrinsic top-down, non-suspended nanowire (Barwicz *et al* 2010) has a piezoresistive factor similar to bulk. Regarding the measurements presented in this paper, the gauge factors extracted are close to the bulk values with the exception of the released low doped nanowire. In fact, in this case, the experiment gives twice the bulk value. Furthermore, the observed increase of the gauge factor with nanowire release is probably due to the change of the surrounding medium. In fact, non-released nanowires are embedded in SiO_2, while released nanowires are in air with the creation of a thin native oxide layer. As mentioned earlier, the surface charge density for nanowires embedded in SiO_2 is at least of the order of 2.84×10^{11} cm^{-2} (Tachi *et al* 2009), while for the case of suspended nanowires it is probably higher. The difference can be attributed to the variation of the oxide quality. The native oxide, formed when the nanowire is exposed to air (suspended nanowire), is of poor quality compared to the BOX present under the non-suspended nanowire. Furthermore, as the native oxide is irregular, a large variation of the surface charge density can be expected. Saying this, the charge trapping in dielectric materials (SiO_2) can influence the observed piezoresistivity of silicon nanowires; it can result in an increase of the measured resistance ('apparent resistance'). It is expected that the influence of the charge trapping process increases with decreasing doping concentration due to the creation of space charge regions inside the nanowire (for doping concentrations close to the intrinsic level). In more detail, the nanowire dopants are accumulated close to the interface of the nanowire with the SiO_2 surrounding it; in this way, the main body of the nanowire is depleted of free carriers and so the resistivity of the device appears higher. Naturally, in this case, the relaxation time constant of the trapping process has to be considered and compared with the duration of an experiment for the determination of the piezoresistive factors. When the relaxation time constant is negligible with respect to the duration of the measurement, there is no danger for the extraction of conclusions. However, when the time constant becomes comparable to the duration of the measurement, one should be careful not to confuse piezoresistive properties with charge depletion effects.

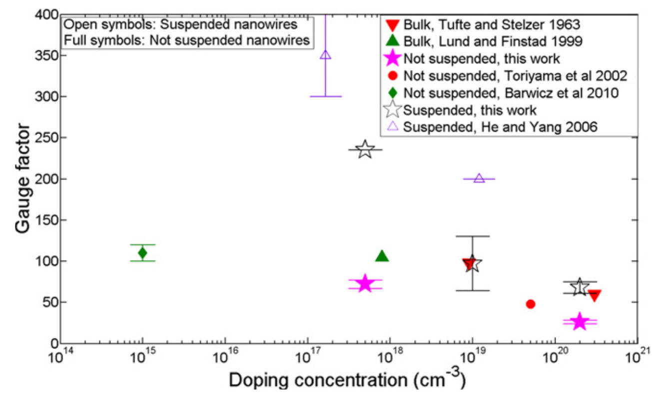

Figure 11. Comparison with previous experimental work (including Tufte and Stelzer (1963), Lund and Finstad (1999) for bulk values). The full triangles correspond to bulk values, the other full symbols correspond to non-suspended nanowires and the open symbols correspond to suspended nanowires. Details of the dimensions are given in table 2.

Table 2. Device dimensions used for gauge factor measurements.

Reference	w (nm)	t (nm)	l (μm)
This work	40	38	0.35–0.8
This work	40	38	0.35–0.8
This work	50	160	2.5
This work	40	38	0.5–5
This work	40	38	0.5
(Toriyama and Sugiyama 2002)	53	53	3
(Barwicz *et al* 2010)	45	45	0.4
(He and Yang 2006)	50	50	—
(He and Yang 2006)	50	50	—

6. Conclusions

Various electrical and electromechanical tests have been performed on silicon top-down nanowires in order to extract the gauge factor and verify the origin of the piezoresistance measured. In particular, the conductance variation during long time intervals was monitored and numerous measurements aiming at reproducibility verification were performed. It has been shown that the resistance increase observed for strained silicon nanowires is a real effect that is not masked by conductance instabilities. Top-down nanowires appear, in general, to have gauge factors close to the bulk values. As the only exception, we can cite a 5×10^{17} cm^{-3} doped suspended nanowire that shows a gauge factor twice as high as the bulk value. Comparison with previous experimental work (Barwicz *et al* 2010, Milne *et al* 2010) situates the piezoresistive coefficients of top-down nanowires much lower than the ones observed for bottom-up devices (He and Yang 2006). In particular, the gauge factor measured for the 10^{19} cm^{-3} doped bottom-up nanowires is twice as high as the one measured for their top-down counterparts. Similarly,

for the 5×10^{17} cm^{-3} structures there is a difference of 1.5–2 times. From this point of view, the results presented here support the work of Milne *et al* (2010) and Barwicz *et al* (2010) where no giant piezoresistance effect was observed. Regarding the impact of nanowire release on the gauge factor, it seems to greatly enhance the piezoresistive effect. In the case of the 5×10^{17} cm^{-3} nanowires an increase of more than 100% is measured. It is actually supposed that the surrounding nanowire medium influences the piezoresistive properties of the device. Based on the assumption of the creation of a depletion width on the nanowire surface, the oxide quality plays an important role in determining the surface charge concentration. The native oxide (suspended nanowires) results in a higher surface charge concentration and thus larger depletion region than thermal and buried oxide (non-released nanowires). In the future, suspended nanowires conceived for electromechanical applications should be passivated either by SiO_2 or by other chemical layers (Haick *et al* 2006).

Acknowledgments

The authors acknowledge financial support from both the European Commission under the FP7 STREP NEMS-IC and the French Research Agency under the Carnot-NEMS research program.

References

Arcamone J, Sansa M, Verd J, Uranga A, Abadal G, Barniol N, van den Boogaart M A F, Brugger J and Pérez-Murano F 2009 Nanomechanical mass sensor for spatially resolved ultrasensitive monitoring of deposition rates in stencil lithography *Small* **5** 176–80

Armigliato A, Nobili D, Ostoja P, Servidori M and Solmi S 1977 Solubility and precipitation of boron in silicon and supersaturation resulting by thermal predeposition *Proc. Electrochemical Society* vol 77–2 *Semicond. Silicon* pp 638–47

Ayari A, Vincent P, Perisanu S, Choueib M, Gouttenoire V, Bechelany M, Cornu D and Purcell S T 2007 Self-oscillations in field emission nanowire mechanical resonators: a nanometric dc–ac conversion *Nano Lett.* **7** 2252–7

Bargatin I, Myers E B, Arlett J, Gudlewski B and Roukes M L 2005 Sensitive detection of nanomechanical motion using piezoresistive signal downmixing *Appl. Phys. Lett.* **86** 133109

Barwicz T, Klein L, Koester S J and Hamann H 2010 Silicon nanowire piezoresistance: impact of surface crystallographic orientation *Appl. Phys. Lett.* **97** 023110

Colinet E, Duraffourg L, Labarthe S, Robert P, Hentz S and Andreucci P 2009a Self-oscillation conditions of a resonant nanoelectromechanical mass sensor *J. Appl. Phys.* **105** 124908

Colinet E *et al* 2009b Ultra-sensitive capacitive detection based on SGMOSFET compatible with front-end CMOS process *IEEE J. Solid-State Circuits* **44** 247

Diarra M, Niquet Y-M, Delerue C and Allan G 2007 Ionization energy of donor and acceptor impurities in semiconductor nanowires: importance of dielectric confinement *Phys. Rev.* B **75** 045301

Feng X L, White C J, Hajimiri A and Roukes M L 2008 A self-sustaining ultrahigh-frequency nanoelectromechanical oscillator *Nature Nanotechnol.* **3** 342–6

Haick H, Hurley P T, Hochbaum A I, Yang P and Lewis N S 2006 Electrical characteristics and chemical stability of non-oxidized, methyl-terminated silicon nanowires *J. Am. Chem. Soc.* **128** 8990–1

He R, Feng X L, Roukes M L and Yang P 2008 Self-transducing silicon nanowire electromechanical systems at room temperature 2008 *Nano Lett.* **8** 1756–61

He R and Yang P 2006 Giant Piezoresistance effect in silicon nanowires *Nature Nanotechnol.* **1** 42–6

Ilic B, Craighead H G, Krylov S, Senaratne W, Ober C and Neuzil P 2004 Attogram detection using nanoelectromechanical oscillators *J. Appl. Phys.* **95** 3694–703

Jensen K, Kim K and Zettl A 2008 An atomic-resolution nanomechanical mass sensor *Nature Nanotechnol.* **3** 533–7

Kanda Y 1982 A graphical representation of the piezoresistance coefficients in silicon *IEEE Trans. Electron Devices* **29** 64–70

Lube T and Manner M 1997 Development of a bending-test device for small samples *Key Eng. Mater.* **132–136** 488–91

Lugstein A, Steinmair M, Steiger A, Kosina H and Bertagnolli E 2010 Anomalous piezoresistance effect in ultrastrained silicon nanowires *Nano Lett.* **10** 3204–28

Lund E and Finstad T G 1999 *InterPACK'99: Pacific RIM/ASME Int. Intersociety Electronics Photonic Packaging Conference* (*Advances in Electronic Packaging*) pp 215–8

Lund E and Finstad T G 2004 Design and construction of a four-point bending based set-up for measurement of piezoresistance in semiconductors *Rev. Sci. Instrum.* **75** 4960–6

Mile E, Jourdan G, Bargatin I, Marcoux C, Labarthe S, Kharrat C, Andreucci P, Hentz S, Colinet E and Duraffourg L 2010 In-plane nanoelectromechanical resonator based on silicon nanowire piezoresistive detection for frequency-shift sensing applications *Nanotechnology* **21** 165504

Milne J S, Rowe A C H, Arscott S and Renner Ch 2010 Giant piezoresistance effects in silicon nanowires and microwires *Phys. Rev. Lett.* **105** 226802

Reck K, Richter J, Hansen O and Thomsen E V 2008 Piezoresistive effect in top-down fabricated silicon nanowires 2008 *MEMS 2008*

Richter J, Pedersen J, Brandbygr M, Thomsen E V and Hansen O 2008 Piezoresistance in p-type silicon revisited *J. Appl. Phys.* **104** 023715

Rowe A 2008 Silicon nanowires feel the pinch *Nature Nanotechnol.* **3** 311–2

Schmidt V, Senz S and Gösele U 2007 Influence of the Si/SiO_2 interface on the charge carrier density of Si nanowires *Appl. Phys.* A **86** 187–91

Seo K, Sharma S, Yasseri A A, Stewart D R and Kamins T I 2006 Surface charge density of unpassivated and passivated metal-catalyzed silicon nanowires *Electrochem. Solid-State Lett.* **9** G69–72

Smith C S 1954 Piezoresistance effect in germanium and silicon *Phys. Rev.* **94** 42–9

Staufer U *et al* 2007 Micro- and nanosystems for biology and medicine *Microelectron. Eng.* **84** 1681

Tachi K *et al* 2009 Relationship between mobility and high-k interface properties in advanced Si and SiGe nanowires *Electron Devices Mtg (IEDM) IEEE Int.*

Toriyama T and Sugiyama S 2002 Single crystal silicon nano-wire piezoresistors for mechanical sensors *J. Microelectromech. Syst.* **11** 605–11

Toriyama T, Tanimoto Y and Sugiyama S 2001 Characteristics of silicon nano wire as piezoresistor for nano electro mechanical systems *IEEE*

Tufte O N and Stelzer E L 1963 Piezoresistive properties of silicon diffused layers *J. Appl. Phys.* **34** 314–8

Yang Y T, Callegari C, Feng X L, Ekinci K L and Roukes M L 2006 Zeptogram-scale nanomechanical mass sensing *Nano Lett.* **6** 583–6

Zhang Y, Liu X Y, Ru C H, Zhang Y L, Dong L X and Sun Y 2011 Piezoresistivity characterization of synthetic silicon nanowires using a MEMS device *IEEE/ASME J. Microelectromech. Syst.* **20** 959–66